Design and Testing of a Multi-Module, Tetherless, Soft Robotic Eel

Robin Hall, Gabriel Espinosa, Shou-Shan Chiang and Cagdas D. Onal[‡]

***Abstract*—This paper presents a free-swimming, tetherless, cable-driven modular soft robotic fish. The body comprises a series of 3D-printed wave spring structures that create a flexible biologically inspired shape that is capable of an anguilliform swimming gait. A three-module soft robotic fish was designed, fabricated, and evaluated. The motion of the robot was characterized and different combinations of actuation amplitude, frequency, and phase shift were determined experimentally to determine the optimal parameters that maximized speed and minimized the cost of transport (COT). The maximum speed recorded was 0.20 BL/s (body lengths per second) with a COT of 15.82. These results were compared against other robotic and biological fish. We operated the robot, untethered, in a variety of environments to test how it was able to function outside of laboratory settings.**

I. Introduction

Robot designs often strive to replicate the motion and attributes of specific animals to match their impressive locomotion capabilities. For example, robots have been created to mimic the undulatory motion of the caudal tail of various fish species. One of the first of these endeavors was the MIT Robotuna in 2003 [1]. Many more designs have been made in a similar manner, by connecting rigid links with motors [2]–[5]. This method relies on the active position control of each link. It increases the active degrees of freedom and body complexity by approximating the smooth flexible motion of a bending body with multiple discrete links.

Researchers have recently turned towards soft materials and actuators as a means of creating more biologically accurate motion. Many use fluidic actuators like hydraulics or pneumatics and soft materials like silicone rubber to create smooth motion [6]–[9]. This approach is much more biologically accurate but can be difficult to manufacture and challenging to control and model. It is also much harder to operate these devices tetherlessly over long periods of time or distance.

In this work, we present a soft robotic fish that bridges the gap between these two design concepts, actuated with servo motors and tendons, yet made predominantly from soft materials (Fig. 1). Building on our previous work [10], we have designed and fabricated a free-swimming modular soft robotic fish with tetherless operation and cable-driven actuation of soft flexible wave-spring sections [11]. The robot is capable of swimming, without any intervention, by bending its long and slender multi-section body in a bio-inspired fish-like swimming gait.

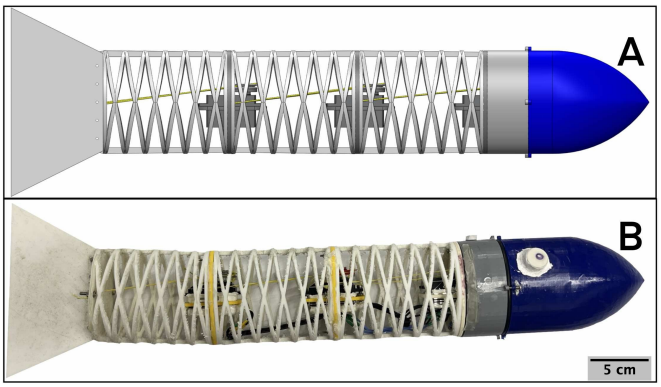

Fig. 1: (A) Cad model of the robot. (B) Physical robot with the addition of a latex skin on the wave spring tail. the three modules are connected together with individual motors to control their motion. The robot's body length was 0.496 m.

The electrical actuation principle simplifies control and the soft body enables smooth, biologically accurate motion. The robot is cable-driven, similar to the tensegrity design seen in other robots [12]–[14]. Unlike these designs, each section of our robot's body is a single, continuous, soft unit. It is able to be driven effectively by cable actuation to generate biologically inspired underwater locomotion gaits.

Fish primarily exhibit undulatory swimming, which is subdivided into four categories: anguilliform, subcarangiform, carangiform, and thunniform. The differences between these modes are derived from the length of the propulsive wave generated down the body, as well as the head-to-tail ratio [15]. Subcarangiform, carangiform, and thunniform swimmers successively decrease the amount of their body used for propulsion. They use roughly half to one-third of their body for maneuvering, and their increased body stiffness limits head motion. This is the primary mode of movement for fish who use their caudal fin for forward thrust like tuna, trout, and many other species [16].

In anguilliform swimming, a traveling wave that increases in amplitude is generated down the length of the whole body pushing water backward, and thereby propelling the fish forward. Animals that use this swimming mode are eels, lampreys, snakes, and worms [17]. Our robot is capable of performing a variety of different swimming gaits, but an anguilliform gait empirically works best for our long, slender, three-module design. Our work is an improvement in the space of bio-robotic eel-like swimmers. We demonstrate how a combination of soft materials and electrical actuation principles can improve upon designs more limited in scope.

*This material is based upon work partially supported by the National Science Foundation (NSF) under Grant Nos. CMMI-1752195, DGE-1922761. Any opinions, findings, and conclusions or recommendations expressed in this material are those of the authors and do not necessarily reflect the views of the NSF.

†The authors are with the WPI Soft Robotics Laboratory, Robotics Engineering Department, Worcester Polytechnic Institute, MA 01609, USA. All correspondence should be addressed to Cagdas Onal cdonal@wpi.edu

The contributions of this work are as follows:

- The design of a soft robotic fish capable of tetherless anguilliform swimming.
- An analysis of the motion and performance of a multi-module robot, as well as a comparison with other biological and robotic anguilliform swimmers.

II. Approach and Methods

The caudal tail of the robot is comprised of three 3D-printed cable-actuated wave spring modules (Fig. 1). In this section, we discuss the robot's design, fabrication, and testing procedures.

A. Modular Wave Springs

The flexible modules and caudal fin were fabricated by fused deposition modeling using Ultimaker Thermoplastic Polyurethane (TPU) filament with a shore hardness of 95A. Each module is an oval wave spring, designed to match the oval-like cross-section of its biological counterpart. The structure is a mesh of diamond-shaped cells formed by two mirrored helices. The wave spring can bend, stretch, and compress, but supports were added down the dorsal and ventral edges of the modules to ensure that only lateral bending is favored as we have presented in [10].

Connected to each flexible module is a rigid servo mount, constructed using Ultimaker Polylactic Acid (PLA). A 20 kg-cm, 0.080 s per 60°-rated servo motor was placed along the lateral line of each module and actuates the bending of the module using a cable and pulley system (Fig. 2). Connected to each servo is a spool with a polyethylene non-elastic braided tendon wound about it. The tendons are kept in tension with two screws on the servo mount of the successive module and for the final module, at the peduncle (base of the fish tail).

In order to maintain biological accuracy and streamlined in-water swimming, a pointed head is attached to one end of the robot. It maintains the oval body shape but is tapered to a point like a teardrop. The head is hollow and houses the control board (Arduino Nano) and a 240 mAh lithium polymer battery. Attached to the peduncle is a caudal fin. In prior work [10], we determined that a 152 mm^2 area, 2 mm thick, trapezoid caudal fin produces the most thrust for oscillatory bending motion (when compared to other regular polygon fin shapes of varying area and thickness). We used this finding as a foundation for the work presented here, only adjusting the aspect ratio for the larger module size. The robot's final body dimensions are an oval with an 84.3-mm major diameter, 49.3-mm minor diameter, and a total body length of 0.496 m. Furthermore, the advances in additive manufacturing and material science have allowed us to fabricate the robot rapidly and cost-effectively using multiple materials with an Ultimaker S5 3D printer.

B. Multi-module Design

The modular design provides the flexibility of performing different locomotion gaits by increasing the number of wave spring modules used in the caudal tail and by adjusting the phase shift between modules. For instance, a single-module tail can only perform an oscillatory pattern, closely resembling thunniform swimming. In contrast, a multi-module tail (three and above) can perform any type of gait including anguilliform swimming.

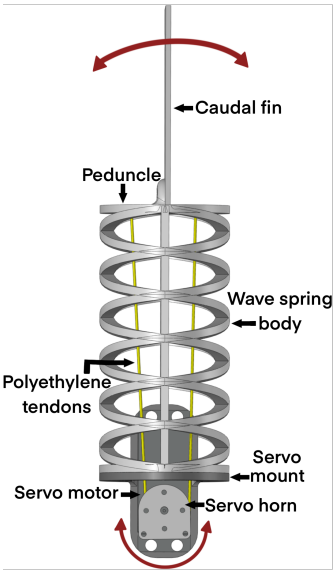

Fig. 2: Top view of the robot demonstrating the tendon-driven actuation mechanism. The tendon is wound around the spool while the servo motor is in its neutral position. Rotating the servo pulls the cables, which bends the wave spring in the lateral direction.

This robot is comprised of three identical modules, chained in series. The dimensions of the robot are similar to European and American Eels (*Anguilla anguilla*, *Anguilla rostrata*), that are on average 60 to 80 cm in length and 4 to 7 cm in height. Robotic actuation methods, like servo motors, are not able to reach the highest frequencies of most thunniform or carangiform swimming fish [18]. However, anguilliform swimmers operate at both lower frequencies and lower speeds [19], which are much closer to the capabilities of our actuation method.

C. Performance Metrics

In order to fully characterize the performance of the robot, the speed and COT were compared at different gait parameters: motor amplitudes, frequencies, and phase shifts. The range of each parameter was set based on the physical limits of the servo motors.

The robot is primarily composed of hollow wave springs which allow water to freely move through the robot. It was hypothesized from observations of biological eels that the addition of skin would help increase the speed of the robot by providing a surface area for water to push against, essentially using the entire body as a fin instead of just relying on the caudal fin. The skin was made from 0.3 mm thick latex with a shore hardness of 40A and had an insignificant effect on the overall dimensions or weight of the robot. It was affixed to each motor mount using the correct fit: not too tight, leading

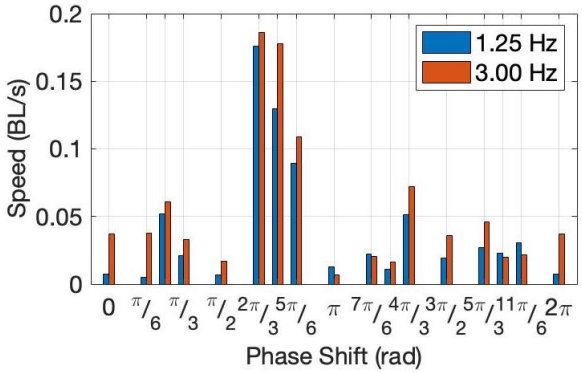

Fig. 3: Speed was recorded for phase-shifted input waves 0 to $^{2\pi}/_{3}$ rad. Biological fish tend to have motion described by a $^{2\pi}/_{3}$ rad phase-shifted traveling wave, thus the increased speed shown at this phase shift on the graph is to be expected. The 3 Hz frequency showed improved performance across nearly all phase shifts tested due to the chosen input amplitude configuration, Configuration 6 (Tab. I).

to restriction of movement, and not too loose that it would mask the lateral movement. We tested various frequencies and other gait parameters with and without the skin and found that the skin increased the speed of the robot significantly.

Energy consumption is critical to our understanding of the efficiency of robots. It is especially important in mobile soft robots to understand and optimize energy consumption as their size tends to constrain the housing or transporting of large and heavy power sources. In this research, COT is used to measure the efficiency of the robot under different parameters. COT is defined as:

$$COT = \frac{P}{mg\bar{v}}, \tag{1}$$

where $P = VI$ is the average power consumption, where V is the average voltage and I is the average current measured throughout the duration of the test, m is mass, g is the acceleration due to gravity, and $\bar{v}$ is the average velocity of the robot for the duration of the test.

An INA219 current monitor was added to measure the power consumption. In order to record the data from the sensor, a cable was used to log the serial monitor of the Arduino. Future work will include wireless communication to both control the robot and collect data, including telemetry and exteroceptive sensing.

D. Experimentation

Testing was conducted in a 1.2x0.45x0.53 m fish tank filled roughly 80% with tap water. Cameras were positioned facing the top and side of the tank. The side view enabled us to record the speed of the robot using PHYSLETS TRACKER [20]. The top view allowed us to record and verify the robot's swimming gait.

The robot has a center of buoyancy at the base of the head, which causes its body to sink. To achieve neutral buoyancy (stabilized at a fixed depth) [21], closed cell foam was added around each motor to increase the buoyant force along the length of the tail, while not impeding the flexibility of each module. 0.2 kg of weight was also added to the sealed head component to counter the buoyant force created by the trapped air inside.

TABLE I: Input amplitude configurations for each fish module during in-water experiments.

Input Amplitude Configuration	Head (°)	Mid (°)	Tail (°)
1	90	90	90
2	80	80	80
3	70	70	70
4	60	60	60
5	50	50	50
6	70	80	90
7	65	75	90
8	60	70	90
9	55	65	90
10	50	60	90

For each experiment, the robot swam 0.5 m in a straight line starting at rest. Once the robot reached the end of the tank, it was moved back to the starting position for the start of the next trial. For each data point, we performed three trials and analyzed all the results in PHYSLETS TRACKER [20]. We found that the robot did not always travel in a perfectly straight line and some trials had to be repeated to ensure the robot was traveling with minimum drift for accurate results.

III. RESULTS AND DISCUSSION

Speed and COT were compared at different motor amplitudes, frequencies, and phase shifts. The maximum speed (0.20 BL/s) and minimum COT (15.82) were achieved at 1.25 Hz, a 90° input amplitude at each module, and a phase shift of $^{2\pi}/_{3}$ rad.

A. Phase Shift

Biological anguilliform swimmers exhibit a traveling wave that moves down the length of the body. We hypothesized that this same method would yield the best performance for our robot. We tested the full range of possible phase shifts from 0 to 2π rad (Fig. 3). Each phase shift was tested at both 1.25 Hz and 3 Hz frequencies in Configuration 6 (Tab. I). In testing, it was found that the only phase shifts resulting in any significant speed were $^{2\pi}/_{3}$ rad to $^{5\pi}/_{6}$ rad and these were tested over three trials with a resulting average standard deviation (STD) of 0.89. The maximum speed of 0.19 BL/s was achieved at $^{2\pi}/_{3}$ rad. For both tested frequencies, the phase shift performance trends were very similar, with 3 Hz performing slightly better due to the chosen input amplitude configuration (studied in detail in the next section). For every amplitude, frequency, and COT test, we used a baseline phase shift of $^{2\pi}/_{3}$ rad.

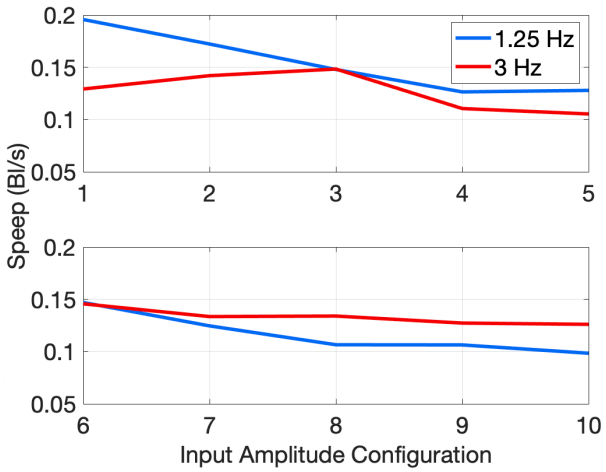

Fig. 4: Speed of the robot was recorded at each input amplitude configuration from Table I. Configurations 3 and 6 are almost equivalent and yielded some of the fastest speeds recorded. The maximum speed of 0.20 BL/s was achieved when each module was set to an amplitude of 90°, Configuration 1.

B. Amplitude

The fish can operate at different amplitudes for each module. Here, we refer to the input amplitude of the servo pulleys, since the output amplitudes vary with load and the location of the module from head to tail. We used two different methods of varying input amplitudes for testing; first, we used the equal amplitude method, keeping all amplitudes uniform and increasing the amplitude by 10°, starting at 50°. In previous work [10], we determined for a single module tail, 90° provided the most forward force. On this robot, the highest speeds were recorded when all modules had an input amplitude of 90°, which was consistent with our previous work.

For longer anguilliform swimmers in nature, the wave generated by their body increases in amplitude from head to tail. To test this, our second method (the increasing amplitude method) set the first module at 50°, the second module at 60°, and the third at 90°. The amplitude of the first two modules was then increased by 5° until the first and second modules reached 70° and 80° respectively. We kept the distal module at 90°. Table I simplifies each input amplitude configuration to single number labels that are used throughout the paper. Higher amplitudes yielded higher speeds, consistent with the equal amplitude method, and overall, the varied amplitude method had lower output speeds.

For each method, the input amplitudes were tested at both 1.25 Hz and 3 Hz for three trials which resulted in an average STD of 0.71. The trends for each frequency were consistent, but 1.25 Hz operated faster for consistent amplitudes and 3 Hz operated faster for varied amplitudes. The fastest speed (0.20 BL/s) was recorded at 1.25 Hz with each module operating with a 90° amplitude (Fig. 4). 0.20 BL/s was the single fastest speed recorded across all the tests, while on average, the maximum speed was 0.16 BL/s.

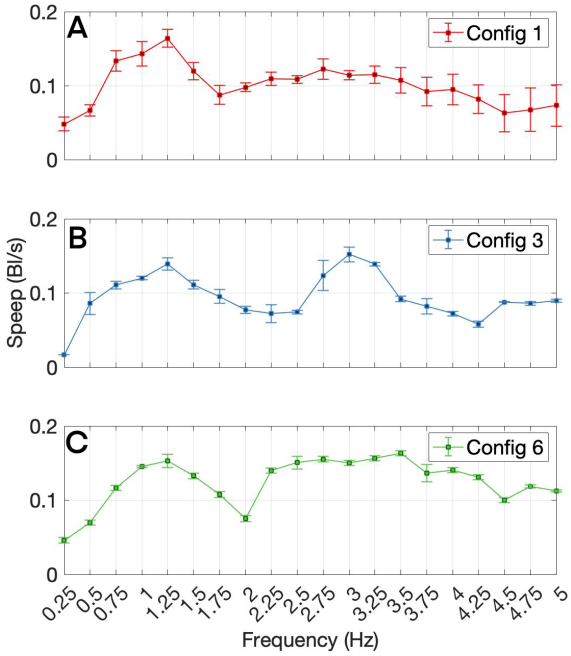

Fig. 5: The speed of the robot was recorded at a range of frequencies from 0.25 Hz to 5 Hz for Configurations 1, 3, and 6. The fastest average speed of 0.16 BL/s was recorded at 1.25 Hz in Configuration 1 (all modules with a 90° input amplitude). The robot did reach 0.2 BL/s in this same configuration but not during these tests.

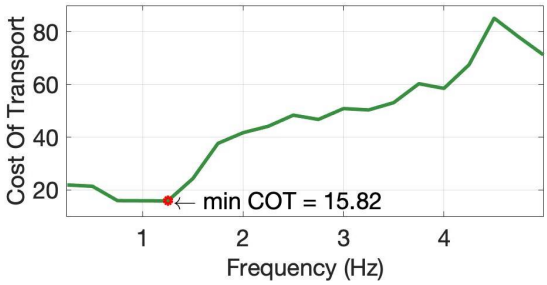

Fig. 6: COT was lowest between 0.75 Hz and 1 Hz, the lowest recorded at 1.25 Hz of 15.82. As frequency increased greater than 1.25 Hz, COT increased significantly as well.

C. Frequency and COT

Frequencies were tested from 0.25 Hz to 5 Hz for three different input amplitude configurations: 1, 3, and 6 (Fig. 5) for three trials resulting in an average STD of 0.01. Two specific ranges resulted in high speeds in each configuration: 0.75 Hz to 1.5 Hz and 2.75 Hz to 3.5 Hz. Configuration 1 yielded the highest average speed of 0.16 BL/s at 1.25 Hz while Configurations 3 and 6 yielded the high speeds at 3 Hz and 3.5 Hz respectively. We used 1.25 Hz and 3 Hz for the remainder of the tests as our baseline frequency.

Visually comparing the motion of the robot under each frequency range, it was also evident that lower frequencies propelled the robot much smoother through the water. The movement was more similar to biological motion and something we will look to quantify in the future.

Frequency had the largest impact on both speed and COT. The lowest COT recorded was 15.82 at 1.25 Hz. COT

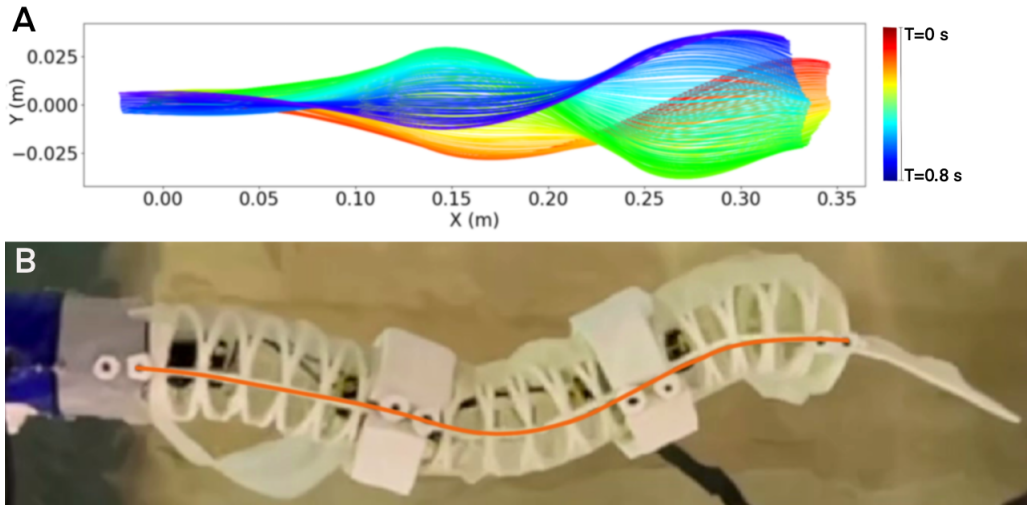

Fig. 7: (A) Clothoid representation of one swimming cycle. The color (ROYGBV) corresponds to the chronological progression of the tail. t = 0 s corresponds to red and t = 0.8 s corresponds to violet. (B) A snapshot of the physical model during the same locomotion experiment with a curve (orange) overlaid to indicate the tracked shape. In water snapshot taken at t = 0.06 s.

increased significantly with frequencies greater than 1.25 Hz, up to 85.2 at 4.5 Hz (Fig. 6). Comparing the two frequency ranges that produced the highest speeds, 0.75 Hz to 1.5 Hz and 2.75 Hz to 3.5 Hz, the former had an average COT of 17.9 and the latter had an average COT of 50.2. This further justified the use of lower frequencies to improve overall performance.

D. Motion Analysis

We analyzed the motion of the robot to verify we were achieving the expected anguilliform swimming gait. The most conventional method of tracking fish body movement is to record the shape of the midline of the tail throughout one actuation cycle [16]. The swimming motion was recorded at 240 fps. We analyzed the motion in PHYSLETS TRACKER.

For analysis, we simplified the robot pose model to piecewise clothoid curves. Clothoid curves, also known as Euler's Spirals or Cornu's Spirals, are curves with linearly varying curvature. The clothoid spiral can be parameterized using the Fresnel integrals. The general parametric form of a clothoid spiral curve is defined as the following:

$$\begin{aligned} x(s) &= x_0 + \int_0^s \cos(\frac{1}{2}\kappa'\tau^2 + \kappa_0\tau + \vartheta_0)d\tau \\ y(s) &= y_0 + \int_0^s \sin(\frac{1}{2}\kappa'\tau^2 + \kappa_0\tau + \vartheta_0)d\tau, \end{aligned} \tag{2}$$

where s is the arc length, $\kappa(t) = \kappa' t + \kappa_0$ is the curvature function with linearly varying curvature, κ_0 is the initial curvature, (x_0, y_0) is the starting point, and ϑ_0 is the initial angle. The angle at arc length s is $\vartheta(s) = \frac{1}{2}\kappa' s^2 + \kappa_0 s + \vartheta_0$.

Using the G^1 Hermite interpolation procedure allowed a plane curve to interpolate two given points with assigned (unit) tangent vectors. We assumed that the curvature of each section was independent of each other on our robot. The G^1 fitting numerical approximation [30] satisfies our need.

The robot operated at 1.25 Hz with each module set to 90° amplitudes with a phase shift of $^{2\pi}/_{3}$ rad, having a total compliant length of 0.42 m from the base of the head to the tail. We used Tracker to obtain the position and orientation (x, y, ϑ) of each module's rigid component for one complete swimming cycle and then used the G^1 fitting algorithm to find the clothoids that fit each section (Fig. 7A). Compared to snapshots of the physical robot (Fig. 7B), clothoids accurately model the compliant tail and verified the existence of a traveling wave of increasing amplitude generated down the length of the body.

Using this method, we were also able to calculate the bend angles of every module throughout the swimming cycle. Module 1 (attached to the head) had a right bend angle (RBA) of 26.4° and a left bend angle (LBA) of 24.1°. Module 2 (middle) had an RBA of 56.7° and an LBA of 44.1°. Module 3 (attached to the tail) had an RBA of 55.0° and an LBA of 52.1°. The observed motion follows a traveling wave pattern and the increase in total amplitude from head to tail is in line with biological examples [16].

Biological anguilliform swimmers exhibit a body wave that increases in amplitude down the length of the tail. Even though we set each module to the same amplitude, we still observed a small increase in amplitude down the length of the robot. We hypothesize this is due to the considerable mass of the head compared to the rest of the tail, which acts as an anchor point. The body geometry and mass distribution may serve a similar role as a form of physical intelligence to generate this increase in wave amplitude in biological anguilliform swimmers. In future work, we will look to vary both the size and mass of the head to study this effect.

E. Performance Analysis

We compared the performance of the robot to other robots capable of anguilliform swimming and a selection of eels, one of the most common biological anguilliform swimmers

TABLE II: Comparison between biological and robot anguilliform swimmers

Name and Source	Speed (BL/s)	Frequency (Hz)	Type	# of Modules	Cost of Transport	Unteathered
Fluid Dielectric Elastomer Eel [22]	0.01	0.33	Soft	3	-	No
SMA Undulating Body [23]	0.02	0.33	Soft	3	-	No
Eel-Like Robot [24]	0.11	3	Rigid	5	-	Yes
Eel-Inspired Robot [25]	0.198	1.25	Soft	4	19.21	No
Wave Spring Eel	0.20	1.25	Soft	3	15.82	Yes
FEA Eel [26]	0.22	0.67	Soft	5	-	No
Amphibious Snake Robot [27]	0.23	0.9	Rigid	8	-	Yes
Anguilla anguilla [19]	0.55	1.25	Bio	-	0.42	-
Anguilla rostrata [28]	0.6	1.25	Bio	-	0.42	-
Anguilla japonica [29]	0.68	1.25	Bio	-	-	-

(Tab. II). The robots selected operated in a similar frequency range (0.33 to 3 Hz) to our robot and also had similar maximum speeds (0.01 to 0.22 BL/s). Our robot had a maximum speed of 0.20 BL/s when operating at 1.25 Hz. This was very similar to some of the selected robots, with ours uniquely able to swim untethered. This could have an impact on our speed compared to the other robots, but is an important feature in the viability of this design.

Although biological eels are capable of swimming at higher frequencies than the robots, there is data available for their swimming speed and COT at 1.25 Hz. A key difference between the performance of our robot when compared to biological eels is a positive linear relationship between frequency and speed [28]. Our robot does not exhibit this linear relationship, limiting its capacity to keep pace with biological eels in all situations. We are also limited by amplitude, with a maximum bending angle of only 56°. In future iterations, we will look to increase both frequency and amplitude to increase the speed of the robot.

Lastly, we also tested the robot in a swimming pool and a lake to determine the robustness of the design outside the controlled fish tank environment. The robot was tested at various depths spanning from 0 to 2 m at the Worcester Polytechnic Institute swimming pool and at Lake Quinsigamond in Worcester, Massachusetts. The robot operated at full capacity in both environments but the closer the robot was to the surface of the water, the more it was impacted by wakes and surface disturbances. Primarily, the heading of the robot was affected, as we currently do not have an active steering method. Snapshots from these tests are seen in Fig. 8 and clips from both environments can be seen in the reference video.

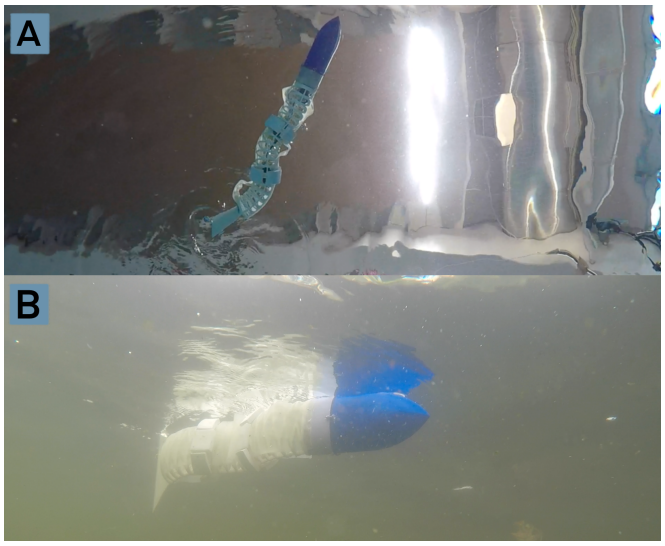

Fig. 8: (A) Robustness testing in Worcester Polytechnic Institute swimming pool and (B) Lake Quinsigamond. The robot is able to operate at depths of 0 to 2 m and can function with disturbances from wake and debris.

IV. Conclusion

We presented a multi-module cable-driven soft robotic fish that is capable of performing open-loop controlled, untethered swimming. The robot was able to execute a biologically accurate anguilliform swimming gait and exhibited a traveling wave that increased in amplitude down the length of the tail. The maximum speed achieved was 0.20 BL/s at 1.25 Hz with a 90° input amplitude at each module and a phase shift of $^{2\pi}/_{3}$ rad. It also had a low COT of 15.82. When compared to other fish robots operating at a low-frequency range, our robot performed very similarly, but more efficiently and untethered. We also compared our robot to biological eels operating at the same frequency and the eels were able to swim roughly twice as fast with a COT that was fraction of ours. We will look to increase our speed while maintaining a low COT to better match the capabilities of biological anguilliform swimmers in future work.

Even though our performance and swimming gait resemble a biological eel, the form of the robot is still closer to that of a long fish. We plan to improve performance by reducing the overall size of the robot and replicating the form of an eel by testing different materials, body structures, and actuation methods. Achieving the same motion with fewer motors will significantly reduce our COT. We will also add closed-loop control to help operate the fish in a variety of environments.

References

[1] Alexandra H. Techet, Franz S. Hover, and Michael S. Triantafyllou. Separation and Turbulence Control in Biomimetic Flows. *Flow, Turbulence and Combustion (formerly Applied Scientific Research)*, 71(1-4):105–118, 2003.

[2] Wai Leung Chan, Taesam Kang, and Young Jae Lee. Experiments and identification of an ostraciiform fish robot. In *2007 IEEE International Conference on Robotics and Biomimetics (ROBIO)*, pages 530–534, December 2007.

[3] Zonggang Li, Liming Ge, Weiqiang Xu, and Yajiang Du. Turning characteristics of biomimetic robotic fish driven by two degrees of freedom of pectoral fins and flexible body/caudal fin. *International Journal of Advanced Robotic Systems*, 15(1):1729881417749950, January 2018.

[4] Donato Romano, Akshat Wahi, Marco Miraglia, and Cesare Stefanini. Development of a Novel Underactuated Robotic Fish with Magnetic Transmission System. *Machines*, 10(9):755, September 2022.

[5] Li Wen, Tianmiao Wang, Guanhao Wu, and Jianhong Liang. Quantitative Thrust Efficiency of a Self-Propulsive Robotic Fish: Experimental Method and Hydrodynamic Investigation. *IEEE/ASME Transactions on Mechatronics*, 18(3):1027–1038, June 2013.

[6] Ardian Jusufi, Daniel M. Vogt, Robert J. Wood, and George V. Lauder. Undulatory Swimming Performance and Body Stiffness Modulation in a Soft Robotic Fish-Inspired Physical Model. *Soft Robotics*, 4(3):202–210, September 2017.

[7] Andrew D. Marchese, Cagdas D. Onal, and Daniela Rus. Autonomous Soft Robotic Fish Capable of Escape Maneuvers Using Fluidic Elastomer Actuators. *Soft Robotics*, 1(1):75–87, March 2014.

[8] Robert K. Katzschmann, Andrew D. Marchese, and Daniela Rus. Hydraulic Autonomous Soft Robotic Fish for 3D Swimming. In M. Ani Hsieh, Oussama Khatib, and Vijay Kumar, editors, *Experimental Robotics: The 14th International Symposium on Experimental Robotics*, Springer Tracts in Advanced Robotics, pages 405–420. Springer International Publishing, Cham, 2016.

[9] Yu-Hsiang Lin, Robert Siddall, Fabian Schwab, Toshihiko Fukushima, Hritwick Banerjee, Youngjoon Baek, Daniel Vogt, Yong-Lae Park, and Ardian Jusufi. Modeling and Control of a Soft Robotic Fish with Integrated Soft Sensing. *Advanced Intelligent Systems*, n/a(n/a):2000244.

[10] Robin Hall and Erik Skorina. The Effect of Design and Control Parameters of a Soft Robotic Fish Tail to Maximize Propulsion Force in Undulatory Actuation. *RAS/EMBS IEEE 9th International Conference on Biomedical Robotics and Biomechatronics*, January 2022.

[11] Erik H. Skorina and Cagdas D. Onal. Soft Hybrid Wave Spring Actuators. *Advanced Intelligent Systems*, 2(1):1900097, 2020.

[12] Jun Shintake, Davide Zappetti, Timothée Peter, Yusuke Ikemoto, and Dario Floreano. Bio-inspired Tensegrity Fish Robot. In *2020 IEEE International Conference on Robotics and Automation (ICRA)*, pages 2887–2892, May 2020.

[13] Bingxing Chen and Hongzhou Jiang. Swimming Performance of a Tensegrity Robotic Fish. *Soft Robotics*, 6(4):520–531, August 2019.

[14] Yong Zhong, Zheng Li, and Ruxu Du. A Novel Robot Fish With Wire-Driven Active Body and Compliant Tail. *IEEE/ASME Transactions on Mechatronics*, 22(4):1633–1643, August 2017.

[15] Valentina Di Santo, Elsa Goerig, Dylan K. Wainwright, Otar Akanyeti, James C. Liao, Theodore Castro-Santos, and George V. Lauder. Convergence of undulatory swimming kinematics across a diversity of fishes. *Proceedings of the National Academy of Sciences*, 118(49):e2113206118, December 2021.

[16] Alexander J. Smits. Undulatory and oscillatory swimming. *Journal of Fluid Mechanics*, 874:P1, September 2019.

[17] Gary B. Gillis. Undulatory Locomotion in Elongate Aquatic Vertebrates: Anguilliform Swimming since Sir James Gray. *American Zoologist*, 36(6):656–665, December 1996.

[18] Gen Li, Hao Liu, Ulrike K. Müller, Cees J. Voesenek, and Johan L. van Leeuwen. Fishes regulate tail-beat kinematics to minimize speed-specific cost of transport. *Proceedings of the Royal Society B: Biological Sciences*, 288(1964):20211601, December 2021.

[19] Kristiaan D'Août and Peter Aerts. A kinematic comparison of forward and backward swimming in the eel Anguilla anguilla. *Journal of Experimental Biology*, 202(11):1511–1521, June 1999.

[20] Tracker Video Analysis and Modeling Tool for Physics Education. https://physlets.org/tracker/.

[21] J. C. Swallow. A neutral-buoyancy float for measuring deep currents. *Deep Sea Research (1953)*, 3(1):74–81, October 1955.

[22] Caleb Christianson, Nathaniel N. Goldberg, Dimitri D. Deheyn, Shengqiang Cai, and Michael T. Tolley. Translucent soft robots driven by frameless fluid electrode dielectric elastomer actuators. *Science Robotics*, 3(17):eaat1893, April 2018.

[23] K. H. Low, Jie Yang, Anjan P. Pattathil, and Yonghua Zhang. Initial Prototype Design and Investigation of an Undulating Body by SMA. In *2006 IEEE International Conference on Automation Science and Engineering*, pages 472–477, October 2006.

[24] Kenneth A. Mcisaac and James P. Ostrowski. Experimental Verification of Open-loop Control for an Underwater Eel-like Robot. *The International Journal of Robotics Research*, 21(10-11):849–859, October 2002.

[25] Dinh Quang Nguyen and Van Anh Ho. Anguilliform Swimming Performance of an Eel-Inspired Soft Robot. *Soft Robotics*, 9(3):425–439, June 2022.

[26] Hui Feng, Yi Sun, Peter A. Todd, and Heow Pueh Lee. Body Wave Generation for Anguilliform Locomotion Using a Fiber-Reinforced Soft Fluidic Elastomer Actuator Array Toward the Development of the Eel-Inspired Underwater Soft Robot. *Soft Robotics*, 7(2):233–250, April 2020.

[27] Auke Jan Ijspeert and Alessandro Crespi. Online trajectory generation in an amphibious snake robot using a lamprey-like central pattern generator model. In *Proceedings 2007 IEEE International Conference on Robotics and Automation*, pages 262–268, April 2007.

[28] Eric D. Tytell and George V. Lauder. The hydrodynamics of eel swimming: I. Wake structure. *Journal of Experimental Biology*, 207(11):1825–1841, May 2004.

[29] Nobuto Fukuda, Toshihiro Yamamoto, Kazuki Yokouchi, Hiroaki Kurogi, Makoto Okazaki, Yoichi Miyake, Tomowo Watanabe, and Seinen Chow. Active swimming and transport by currents observed in Japanese eels (Anguilla japonica) acoustically tracked in the western North Pacific. *Scientific Reports*, 12(1):3490, March 2022.

[30] Enrico Bertolazzi and Marco Frego. G1 fitting with clothoids. *Mathematical Methods in the Applied Sciences*, 38(5):881–897, 2015.